EMS: Biomedical Sciences
University of Edinburgh
Honours Project

Neuroscience
2019-20

[B097956]
[183]

[Synthesis of a computational biochemical model of hippocampal early long-term plasticity]

Laboratory / Clinical Project
[4994]

BIOMEDICAL TEACHING ORGANISATION

Retention of course work form

With your consent and with your name removed, your dissertation may be retained by the Deanery of Biomedical Sciences for 10 years and made available to other students. Note however that we cannot anonymise video recordings. This collection of work is held to assist future students and you may have used this resource in planning your own projects. If you do not consent to your work being retained, please specify this below and we will destroy the work in accordance with Taught Assessment Regulation 49.

https://www.ed.ac.uk/files/atoms/files/taughtassessmentregulations.pdf

If in future you wish to withdraw consent, please email bmto@ed.ac.uk

Please select one of the following options

I consent to my work being retained and made available to future students. 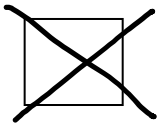

I do NOT consent to my work being retained and made available to future students. ☐

My work contains video recording and I understand that it might be retained and made available to future students. I consent to this with full understanding that it cannot be anonymized. ☐

Table of contents

Abbreviations

LTP	Long-term potentiation
LTD	Long-term depression
HFS	High-frequency stimulation
LFS	Low-frequency stimulation
PSD	Postsynaptic density
AMPAR	α-amino-3-hydroxy-5-methyl-4-isoxazolepropionic acid receptor
AMPARp	Phosphorylated AMPAR
NMDAR	N-methyl-D-aspartate receptor
CaM	Calmodulin
CaMKII	Ca^{2+}/calmodulin-dependent protein kinase II
CaMKIIa	Active CaMKII
PP1	Protein phosphatase 1
PP1a	Active PP1
PP2B	Protein phosphatase 2B (also referred to as calcineurin)
PKA	Protein kinase A
DARPP-32	Dopamine and cAMP-regulated neuronal phosphoprotein (also D)
Dp	Phosphorylated DARPP-32

Abstract

Early long-term potentiation (LTP) and depression (LTD) are forms of plasticity lasting 1-3 hours. Early plasticity relies on Ca^{2+} entry into the postsynaptic space via N-methyl-D-aspartate receptors (NMDARs) following excitation. Ca^{2+} activates the calcium-modulated protein calmodulin, that drives LTP and LTD. High frequencies of Ca^{2+} entry into the cell will favour Ca2+/calmodulin-dependent protein kinase II (CaMKII) activation, whereas lower frequencies will favour protein phosphatase 2B (PP2B/calcineurin) activation by calmodulin. In turn, PP2B activates protein phosphatase 1 (PP1), that negatively regulates CaMKII activity.

At the postsynaptic membrane, α-amino-3-hydroxy-5-methyl-4-isoxazolepropionic receptor (AMPAR) phosphorylation increases in LTP, by CaMKII phosphorylation, and decreases in LTD, by PP2B and PP1 dephosphorylation. This study presents a computational biochemical model of hippocampal early plasticity using COPASI. The model demonstrates that PP2B, PP1 and CaMKII, and their associated pathways, modulate AMPAR phosphorylation in a Ca^{2+} frequency-dependent manner. A bistable behaviour of AMPAR phosphorylation is achieved by grading Ca^{2+} frequency stimulation. AMPAR phosphorylation serves as a readout of LTP and LTD, where high and low AMPAR phosphorylation levels are observed respectively. Future studies can build on this model by fine-tuning the frequency values that elicit LTP/LTD to match those in the literature, completing the biological accurateness of the model.

Lay Abstract

The brain encodes information by modulating synaptic strength, a process known as plasticity. Plasticity varies in form and duration across the brain. In the hippocampus, early plasticity, lasting 1-3 hours, is driven by Ca^{2+} ions entering dendritic spines via N-methyl-D-aspartate receptors (NMDARs) after an excitatory stimulus. The frequency with which Ca^{2+} enters the postsynaptic space determines whether the synapse is strength ened or weakened. Ca^{2+} achieves its effects by binding to proteins in the postsynaptic spine. Two important protein classes addressed in this study are kinases, particularly the Ca2+/calmodulin-dependent protein kinase II (CaMKII), that phosphorylate downstream targets, and phosphatases, particularly protein phosphatase 2B (PP2B/calcineurin) and protein phosphatase 1 (PP1), that dephosphorylate and deactivate their substrates. CaMKII contributes to strengthening synapses by phosphorylating α-amino-3-hydroxy-5-methyl-4-isoxazolepropionic receptors (AMPARs), whereas PP1 and PP2B weaken synapses by dephosphorylating AMPARs. This study develops a computational biochemical model of early plasticity in the hippocampus by using the software COPASI. The model shows that phosphatases and kinases differentially regulate their activity and AMPAR phosphorylation based on Ca^{2+}

frequency entry into the spine. This model serves as a building-block for future models that aim to reproduce early synaptic plasticity using experimental plasticity induction frequencies.

1 Introduction

1.1 Plasticity forms and classification

The brain develops its connectivity and encodes learning and memory by modulating neuronal circuits and synapse strength, a process known as synaptic plasticity (Abbott and Nelson, 2000). The persistence of molecular changes at synapses after neuronal stimulation has ceased leads to two categories of plasticity: long-term potentiation (LTP) and long-term depression (LTD), characterized by strengthening and weakening of synapses respectively (Citri and Malenka, 2008).

Long-term plasticity mechanisms vary across and within brain regions, depending on the induction mechanism, the longevity of synapse strength variation and the molecular pathways involved (Piochon *et al.,* 2016). For example, sustained phosphatase activity, namely that of calcineurin, triggers LTD in the hippocampus (Mulkey *et al.*, 1994), whereas, at Purkinje cell synapses in the cerebellum, it leads to LTP (Schonewille *et al.*, 2010). Additionally, the direction of plasticity, whether it is potentiation or depression, can be controlled by low (~1-10 Hz) or high (~50-100 Hz) frequency stimulation (LFS, HFS) (Albensi *et al.*, 2007).

Plasticity classification also depends on the postsynaptic receptors that mediate it. In the hippocampus, both N-methyl-D-aspartate receptors (NMDARs) and metabotropic glutamate receptors (mGluRs) elicit LTD, where the mGluR pathway stabilizes LTD by protein synthesis (Gladding *et al.,* 2009). The requirement of protein synthesis is indicative of late long-term plasticity, that lasts at least 24 hours after induction, whereas early long-term plasticity is protein synthesis independent and lasts 1-3 hours, mediated by NMDARs (Baltaci *et al.,* 2019).

Fast neuronal excitation is mainly induced by glutamate binding to α-amino-3-hydroxy-5-methyl-4-isoxazolepropionic receptors (AMPARs) on the postsynaptic membrane. The trafficking of AMPARs to and from the synapse determines the magnitude and direction of plasticity (Anggono and Huganir, 2012). AMPAR density and distribution at neighbouring synapses can also affect plasticity expression at a given synapse (Antunes and Simoes-de-Souza, 2018). This phenomenon is known as heterosynaptic plasticity, where synapses that are not directly excited are modulated by strong neighbouring synaptic activity. Conversely, homosynaptic plasticity is characterized by changes in synapses that are directly activated (Chistiakova *et al.*, 2015).

1.2 Modelling hippocampal early homosynaptic plasticity

The challenge of modelling long-term plasticity does not solely arise from plasticity variations across the brain, but from which molecules to focus on. The postsynaptic density (PSD) of mammals is composed of up to a thousand proteins, that include kinases and phosphatases, receptors and scaffolding proteins, among others (Kaizuka and Takumi, 2018). Figure 1 depicts six essential postsynaptic proteins involved in early long-term plasticity: AMPARs, NMDARs, Ca2+/calmodulin-dependent protein kinase II (CaMKII), calcineurin (PP2B) and protein phosphatase 1 (PP1).

Early long-term plasticity in the hippocampus is NMDAR-dependent, relying on Ca^{2+} entry into the PSD, following Na^{+} influx via AMPARs (Citri and Malenka, 2008). An early study showed pharmacological blockade of NMDARs by D-AP5 and Ca^{2+} buffering, by BAPTA, hindered LTD and LTP (Malenka and Nicoll, 1993), prompting the investigation of how two opposing processes appear to share the same mechanism. The answer partially lies in the nature of the Ca^{2+} signal and the intracellular targets of Ca^{2+} (Li *et al.,* 2012). Postsynaptically, calcium binds to the calcium-sensor calmodulin at four distinct sites, altering its affinity for downstream targets depending on the number and site of ions bound (Westerlund and Delemotte, 2018). Calmodulin modulates PP2B and CaMKII activity based on the frequency of the calcium signal (Li *et al.,* 2012). Once CaMKII is active (CaMKIIa), it sustains its activation by autophosphorylation, leading to LTP by phosphorylating AMPARs (Lisman *et al.,* 2002). Contrarily, PP2B activation generates LTD by dephosphorylating AMPARs (Kim and Ziff, 2014) and DARPP-32, releasing the PP1 inhibition (Mulkey *et al.*, 1994). Additionally, active PP1 (PP1a) dephosphorylates CaMKIIa and phosphorylated AMPARs (AMPARp), promoting LTD (Nicoll *et al.,* 2006).

Phosphorylation of the GluR1 subunit of AMPARs, involved in AMPAR trafficking (Anggono and Huganir, 2012), is key for LTP and LTD expression, as demonstrated in mouse models with mutated phosphorylation sites on the GluR1 subunit (Lee *et al.*, 2003). Phosphorylation and dephosphorylation of the GluR1 subunit is governed primarily by CaMKII and the phosphatases PP1 and PP2B (Woolfrey and Dell'Acqua, 2015). This modelling study will focus on the fundamental interplay of CaMKII, PP1 and PP2B in early synaptic plasticity in the hippocampus, at a single dendritic spine/synapse.

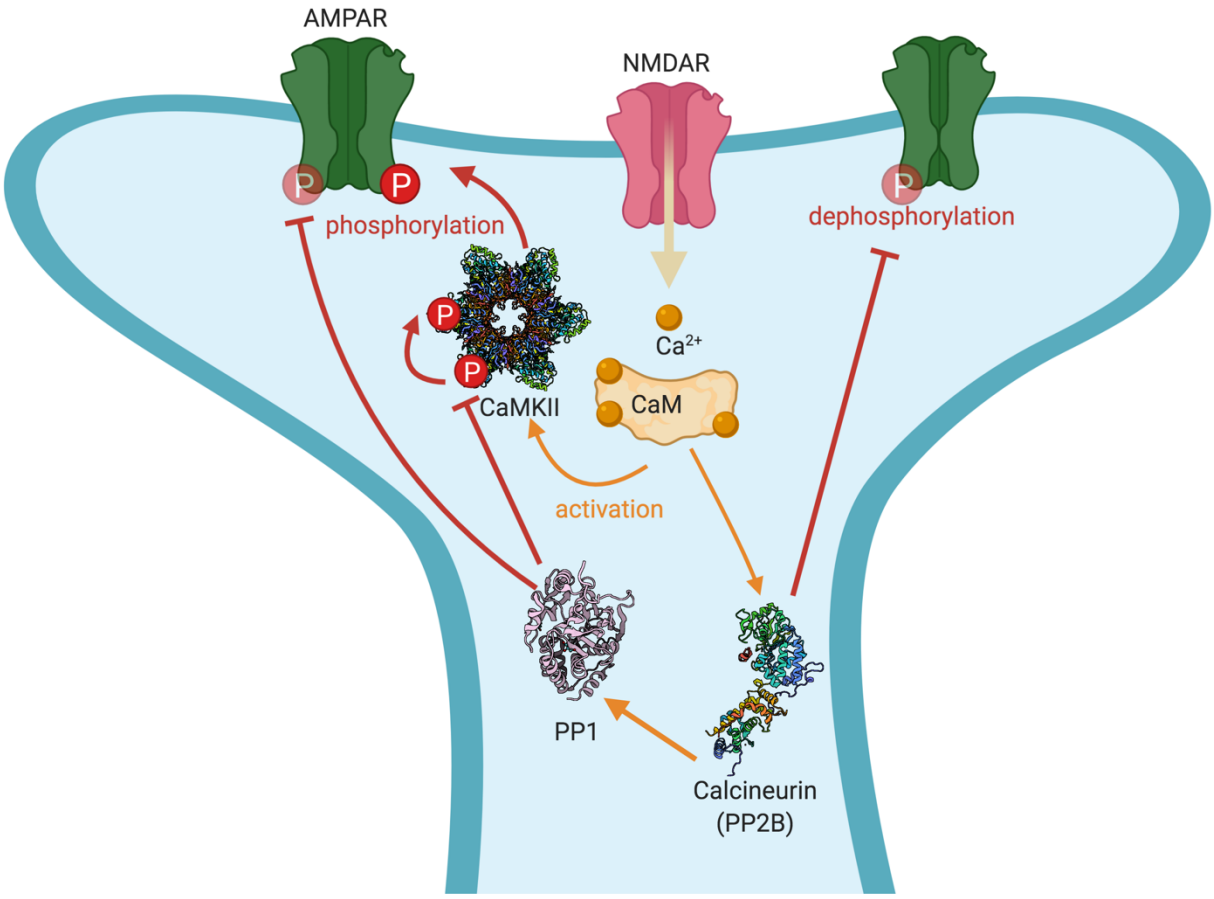

Figure 1. Single spine homosynaptic early plasticity mechanism. The depolarization of the spine by AMPARs leads to Ca^{2+} influx from NMDARs. Ca^{2+} binds to calmodulin (CaM) at four different sites. The number of Ca^{2+} ions bound to calmodulin defines its affinity to selectively activate calcineurin (PP2B) or CaMKII. Once CaMKII is activated, it can sustain its activation by autophosphorylation and it also phosphorylates AMPARs. When calcineurin is activated it can: 1. Dephosphorylate AMPARs; 2. Dephosphorylate and deactivates DARPP-32 (not shown in figure, inactivates PP1) to release the inhibition on PP1. PP1 can then: 1. Dephosphorylate and inactive CaMKII; 2. Dephosphorylate AMPARs. (Li *et al.,* 2012). Figure by author created in the BioRender App.

1.3 Plasticity defects in disease: SynGAP

Constructing a parsimonious model of early plasticity is crucial to study diseases where this process is disrupted, such as autism spectrum disorders (ASD) or schizophrenia. Mutations in the SYNGAP1 gene can lead to intellectual disability, ASD or schizophrenia phenotypes (Gamache *et al.,* 2020). The SYNGAP1 gene encodes the synaptic GTPase-activating protein (SynGAP), that forms complexes with NMDARs and is phosphorylated by CaMKII (Wang *et al.,* 2014). When phosphorylated by CaMKII, SynGAP dissociates from the NMDAR complex and disperses from the PSD, allowing AMPAR trafficking and clustering at the synapse, enhancing LTP (Araki *et al.*, 2015). Electrophysiological studies demonstrate that heterozygote SynGAP mutations cause significantly reduced LTP in hippocampal CA1 neurons compared to wild-type mice (Komiyama *et al.*, 2002). A detailed model englobing AMPARs, CaMKII and phosphatase interaction in hippocampal plasticity

could help investigate alternative pathways that indirectly modulate SynGAP, targeting these pathways to rescue disease effects.

1.4 Aims and hypothesis

The objective when constructing a biochemical model is to balance simplicity and biological accuracy. To achieve this goal, this dissertation focuses on a particular type of homosynaptic plasticity: hippocampal NMDAR and frequency-dependent early plasticity. Detailed modelling of a narrow window of the plasticity spectrum should not be viewed as a limitation, but as an advancement towards creating a building-block that more general models can implement.

This study tests the hypothesis that AMPAR phosphorylation, mediated by CaMKII, PP1, PP2B and their associated molecular pathways, is sufficient to model hippocampal early LTP and LTD. To test the hypothesis, the project aims to:

a) Construct a biochemical model using AMPARp as readout of plasticity.
b) Validate the model by testing it against experimental induction protocols.

2 Methods

For this work, I combined, adapted and extended two biochemical mathematical models of calcium-induced early plasticity (Li et al., 2012; Xie et al., 2019) running all simulations on the resulting model. The model was constructed and tested using COPASI Version 4.27 and the simulation data was visualized and analysed in Python version 3.7. The Python scripts and COPASI model versions are available on GitHub (https://github.com/naimaeb/Early_plasticity_modelling/tree/master).

2.1 Model description

The model was adapted from the Li *et al.,* (2012) model by adding AMPAR phosphorylation and dephosphorylation reactions from the Xie *et al*., 2019 model. The initial concentrations and reaction rates (Table 1) are hippocampal (Li *et al.,* 2012). A minor correction was added to the “Ca_spikes” function taken from the Li *et al*., (2012) model.

In the model (Figure 2), Ca^{2+} enters the spine in spike trains, the number of spikes, frequency an amplitude can be modified. Ca^{2+} binds to calmodulin, that can exist in a relaxed (R) or tense (T) conformation (Stefan *et al.,* 2008). Calmodulin can bind four Ca^{2+} ions, and each binding site is considered separately. Calmodulin can transition from the T to the R state and vice versa, depending

on the number of ions bound. Ca^{2+} binds weakly to calmodulin in the T state and strongly in the R state. R-calmodulin binds and activates PP2B and CaMKII. CaMKII prolongs its activity, independent of R-calmodulin, by autophosphorylation, in turn phosphorylating the GluR1 subunit of AMPARs. PKA phosphorylates and activates DARPP-32, allowing it to bind and inhibit PP1. PP2B dephosphorylates the GluR1 subunit of AMPARs and DARPP-32, releasing PP1 inhibition. Active PP1 dephosphorylates the GluR1 subunit of AMPARs and inactivates CaMKII.

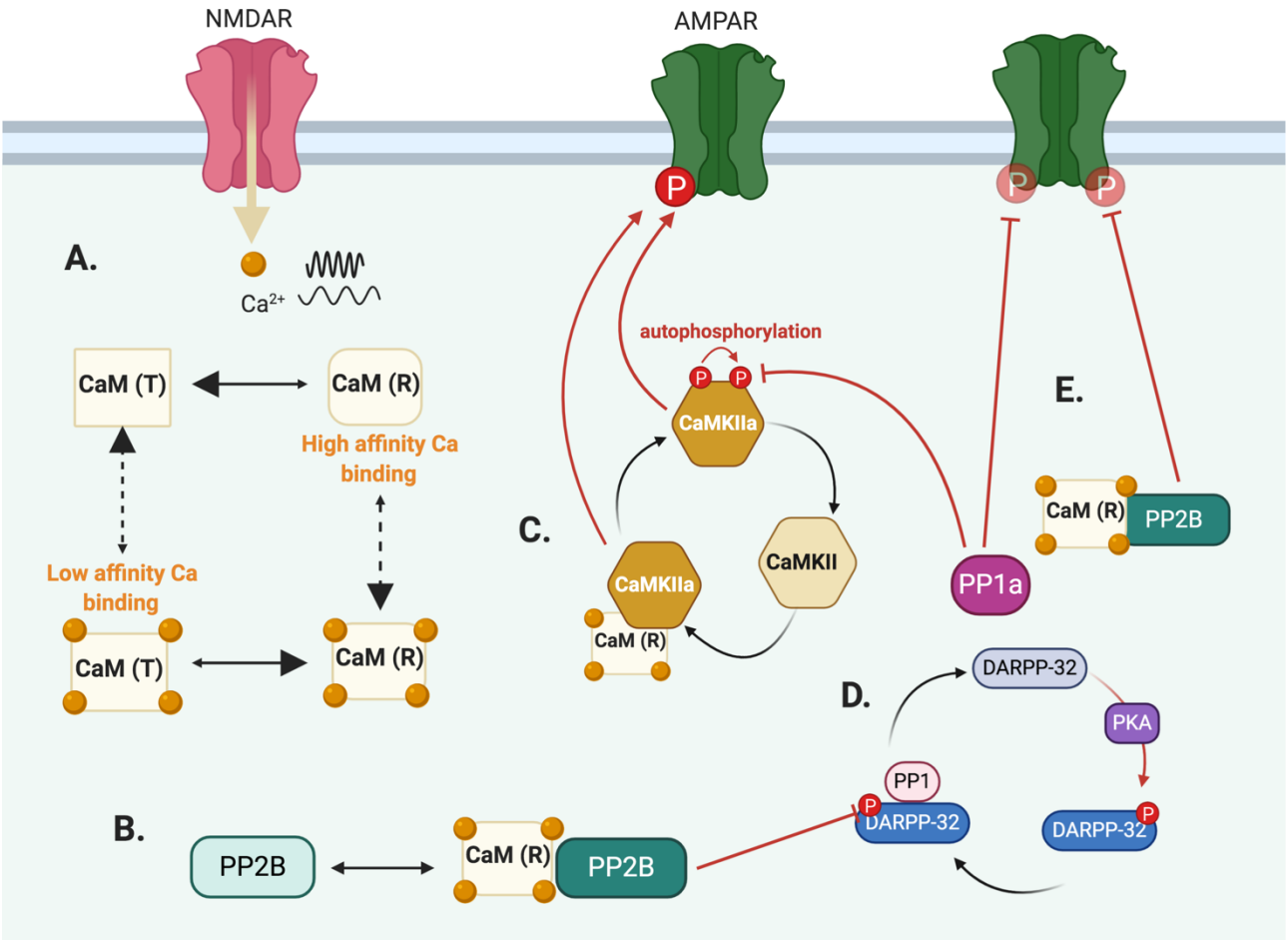

Figure 2. Detailed model description. This figure builds on Figure 1 and it combines two models (Li *et al.,* 2012; Xie *et al.*, 2019). (A) Ca^{2+} enters the spine in trains of spikes of different frequency. Calmodulin exist in two states: tense (T) and relaxed (R). CaMR has a higher binding affinity for calcium than CaMT, the conformational change from the R to the T state is favoured when less calcium is bound and the opposite occurs for high calcium binding. (B) CaMR binds and activates PP2B and CaMKII. (C) CaMKII activated by CaMR can sustain its activation by autophosphorylation, without CaMR. Active CaMKII can then phosphorylate the GluR1 subunit of AMPARs. (D) DARPP-32 is phosphorylated and activated by PKA. Phosphorylated DARPP-32 binds and inhibits PP1. CaMR-bound PP2B (active) dephosphorylates DARPP-32, releasing the inhibiton on PP1. (E) Active PP1 dephosphorylates CaMKIIa and can deactivate it, depending on its degree of phosphorylation. PP1a and calmodulin-bound PP2B dephosphorylate the GluR1 subunit of AMPARs. Figure by author created in the BioRender App.

Table 1: Initial concentrations of species and reaction constants in the model. All values were taken from the Li *et al.,* (2012) curated model on the EBML data base (https://www.ebi.ac.uk/biomodels-main/BIOMD0000000628) unless specified. The reaction constants and species (94 in total) for the different calmodulin states can be found in the model on GitHub.

	Initial value
Species concentration (M)	
AMPAR (unphosphorylated) *(Xie et al., 2019)*	1.49×10^{-6}
AMPARp (phosphorylated) *(Xie et al., 2019)*	1.66×10^{-6}
CaMKII	7.0×10^{-5}
PP2B (calcineurin)	6.0×10^{-6}
PKA	1.2×10^{-8}
PP1	2.0×10^{-6}
DARPP-32	3.0×10^{-6}
CaM (R)	1.45×10^{-9}
CaM (T)	3.0×10^{-5}
Ca^{2+} (basal concentration)	1×10^{-8}
Reaction constants	
CaMKII autophosphorylation (Thr286)	$k = 0\ s^{-1}$ (value changes throughout the simulation); $k_{max} = 6.3\ s^{-1}$
D phosphorylation by PKA (Thr34)	$k_{cat} = 2.7\ s^{-1}$; $k_{off} = 10.80\ s^{-1}$; $k_{on} = 5.6 \times 10^{-6}\ M^{-1}s^{-1}$
Dp dephosphorylation by PP2B (Thr34)	$k_{cat} = 0.2\ s^{-1}$; $k_{off} = 6.4\ s^{-1}$; $k_{on} = 4.1 \times 10^{-6}\ M^{-1}s^{-1}$
Dp inhibits PP1 (by binding)	$k_{off} = 0.4\ s^{-1}$; $k_{on} = 4.0 \times 10^{-6}\ M^{-1}s^{-1}$
CaMKII dephosphorylated by PP1 (Thr286)	$k_{cat} = 2.0\ s^{-1}$; $k_{off} = 0.5\ s^{-1}$; $k_{on} = 3.0 \times 10^{-6}\ M^{-1}s^{-1}$
GluR1 subunit of AMPARs dephosphorylation by PP1	$k_{cat} = 0.35\ s^{-1}$; $K_M = 2 \times 10^{-6}$ M (Xie *et al.*, 2019)
GluR1 subunit of AMPARs dephosphorylation by PP2B	$k_{cat} = 2.0\ s^{-1}$; $K_M = 2 \times 10^{-6}$ M (Xie *et al.*, 2019) (The same value as the K_M from PP1)
GluR1 subunit of AMPARs phosphorylation by CaMKII	$k_{cat} = 0.5\ s^{-1}$; $K_M = 9.0 \times 10^{-5}$M (Xie *et al.*, 2019)
Spine volume	10^{-15} l

Prior to Ca^{2+} stimulation, all parameters were allowed to reach equilibrium, previously determined to be at 800 seconds (Li *et al.,* 2012) and corroborated by running the model and monitoring kinase, phosphatase and receptor concentration values.

The reactions follow mass action kinetics and the systems of reaction equations were solved using the Deterministic (LSODA) COPASI method. All reaction equations were linear ordinary differential equations (ODEs), except CaMKII autophosphorylation which is described by a non-linear ODE. A list of all the ODEs for the systems reactions can be found in the model file on GitHub. The time interval size utilized was of 10^{-3} s.

2.2 Frequency parameter scans

To test how the model behaves as a function of Ca^{2+} input frequency, parameter scans over Ca^{2+} spike frequency (0.1- 200 Hz, logarithmic scale) were performed. Ca^{2+} stimulation was comprised of 1 train of 100 spikes, each spike having the same input of 34650 molecules, leading to intracellular Ca^{2+} maximal levels of 0.7 μM (Li *et al.,* 2012). The scan readouts look at active phosphatase, kinase and receptor concentrations as a function of time.

2.3 Kinase and phosphatase plasticity model

Initially, kinase and phosphatase activation was used as a proxy to measure plasticity. Following the approach of Li *et al.*, (2012), a frequency scan was run for 120 s after stimulus initiation. The activity of individual enzymes was calculated by numerically integrating the concentration as a function of time using the trapezoidal rule:

$$\mathrm{aa(enzyme)} = \frac{\Delta t}{2} \times \left(c(t_0) + 2c(t_1) + 2c(t_2) + \cdots + c(t_n)\right); (1)$$

$$\text{where } n = \frac{\text{total simulation time}}{\Delta t}$$

In equation (1), *aa()* denotes the activated area, Δt is the time interval size, $c(t_k)$ is the concentration of the active enzyme at the k^{th} time step and *n* is the total number of intervals.

Baseline activation was subtracted from the enzyme activated area for each frequency value. The activated area was then multiplied by the catalytic constant of the reaction of the enzyme acting on the GluR1 subunit of AMPARs (k_{cat}_enzyme). The difference between kinase (CaMKII) and

phosphatase (PP1 and PP2B) activity was used to determine the direction of plasticity, using 0.1Hz as the baseline. The activity difference for each frequency was calculated by:

$$\text{activity difference}_{\text{j}} = k_{cat}CaMKII * \text{aa(CaMKII)}_j - k_{cat}PP2B * \text{aa(PP2B)}_j - k_{cat}PP1 * \text{aa(PP1)}_j - \text{activity difference}_{0.1}; (2)$$

where j is a given simulation frequency

If the activity difference is negative or positive the readout is interpreted to be LTD or LTP respectively.

2.4 AMPAR phosphorylation plasticity model

The alternative readout used for plasticity is AMPAR phosphorylation, modelled by adding phosphorylation and dephosphorylation reactions from the Xie *et al*., (2019) model of hyperpolarisation-gated synaptic plasticity. A modification was added to the original reactions, as the catalytic constant for AMPAR dephosphorylation by PP1a and phosphorylation by CaMKIIa were equal. In this model, the k_{cat} for PP1a dephosphorylation of AMPARs was 0.35 s^{-1} as in Li *et al*., (2012).

AMPAR phosphorylation was measured for 26 or 30 minutes from stimulation induction, in accordance with experimental evidence of early plasticity maintenance (Baltaci *et al.,* 2019). Phosphorylation was quantified with respect to baseline values.

2.5 Plasticity stability

To investigate phosphorylation and dephosphorylation balance, parameter scans were run for the catalytic constant of CaMKIIa dephosphorylation by PP1a ($k_{cat}^{CaMKIIp\_PP1}$) (0.15 to 0.5 s^{-1}). AMPARp stability was used as a readout, after 1600 s, to quantify the required strength of phosphorylation and dephosphorylation needed to mimic early plasticity for a range of frequencies (0.1 – 200 Hz).

The second version of the model on GitHub includes PP2B dephosphorylation of AMPARs. The shared terms between PP1a and CaMKIIa are removed, when acting on AMPARs. No simulations were run on this model due to time constraints.

2.6 Model validation

The model was tested with the plasticity induction protocols in Table 2. Furthermore, the model and data analysis code were verified by successfully replicating figures form Xie *et al*., (2019) and Li *et al.,* (2012).

Table 2: Plasticity induction protocols: The following protocols are experimental and correspond to electrophysiological hippocampal stimulation, not direct Ca^{2+} entry into a spine.

Plasticity type	Induction protocol	Reference
Early LTP (1-3h)	1 train; 100 pulses; 100Hz (1s)	(Vertes, 2005)
Early LTD (15 min)	1 train; 900 pulses; 1 Hz (15 min)	(Albensi and Mattson, 2000)
Early LTD (30 min); stronger LTD than when applying the same protocol with 600-900 pulses.	1 train; 1200 pulses; 1 Hz (20 min) 2 trains; 600 pulses; 1 Hz (10 min stimulation, 10 min separation)	(Mockett *et al.,* 2002)
Early LTD (30 min)	1 train; 1800 pulses; 3 Hz (10 min) 2 trains; 900 pulses; 3 Hz (5 min stimulation, 10 min separation)	(Mockett *et al.,* 2002)

3 Results

There is no error in the simulations/experiments because the model is deterministic, as opposed to stochastic. In other words, running the same experiment *N* times would always yield the same result. Therefore, there is no need for statistical analysis to assess significance.

3.1 System equilibrium

To correctly analyse results from simulations, the system must first reach equilibrium without any external input, such as Ca^{2+} spikes. Previous modelling determined equilibrium time to be at 800 s (Li *et al.,* 2012) and it was replicated in the current model (Figure 3). Although the analysis of when equilibrium was reached was qualitative, it can be argued that the system will not fluctuate further once it has plateaued if there is no input added.

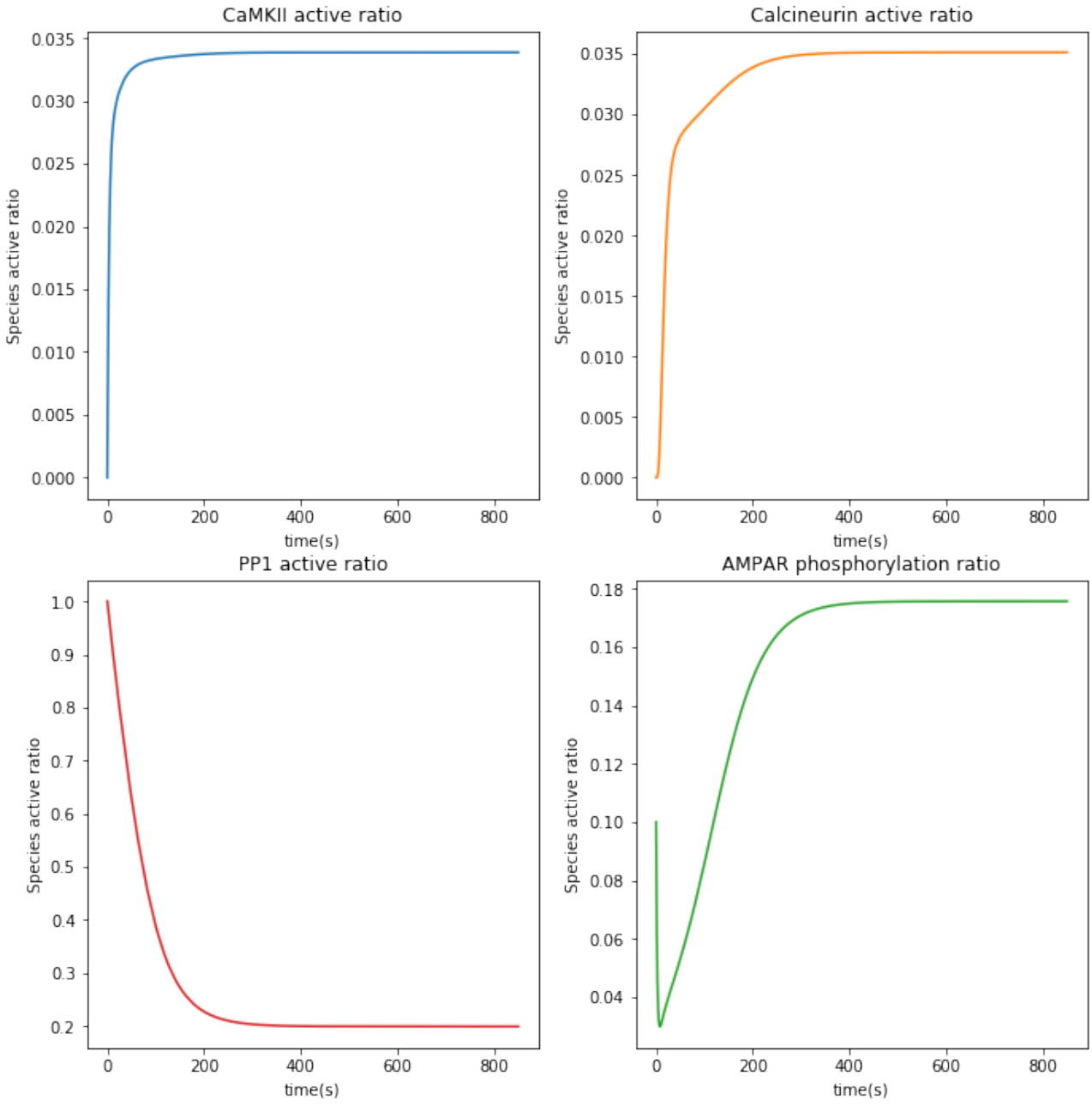

Figure 3. Model equilibrium analysis. (Clockwise, from top left) Temporal variation of four different activated species ratio (CaMKII, PP2B/calcineurin, PP1 and phosphorylated AMPARs). Equilibrium is reached after 400 s, but, to ensure the system has plateaued, it is considered to be at 800 s. This simulation was run without Ca^{2+} spiking or any other stimulus. Initial values before future stimulation (after 800 s) were determined to be (A) 0.034; (B) 0.035; (C) 0.199; (D) 0.176.

3.2 Kinase and phosphatase balance

The activation profiles of PP2B, PP1a, CaMKIIa and AMPARp are displayed in Figure 4, for an LFS (1.43 Hz) and an HFS (43.73 Hz) simulation. Following the approach of Li *et al*., (2012), one can determine the direction of plasticity by: i) looking at the activation ratio of calcineurin and CaMKII or ii) subtracting cumulative activity of phosphatases from kinase. Following LFS, one would expect to see predominant phosphatase activity, whereas after HFS, kinase activity should outweigh that of phosphatases. This shift should yield synaptic depression for LFS and potentiation for HFS, with an intermediate frequency that defines the threshold of transition from LTD to LTP.

When LFS is applied to the spine (Figure 4A), PP1a rises for the duration of the stimulation and then decays. Similarly, PP2B rapidly rises and plateaus for the stimulus duration. Conversely, CaMKIIa and AMPARp remain near baseline level. This behaviour is in accordance with theoretical and experimental evidence, where lower Ca^{2+} concentrations will activate PP2B instead of CaMKII, driving activation of PP1 by PP2B (Colbran, 2004). As described above, AMPAR phosphorylation is reliant on CaMKIIa and inversely proportional to phosphatase activation, thus the results demonstrate the expected behaviour. HFS of the spine (Figure 4B) causes PP2B activity to spike for the duration of the stimulus and then rapidly decay, whereas activity of PP1 and CaMKII rises and is maintained up to 80 s post-stimulation. Nevertheless, CaMKII activity is expected to last for an hour after LTP induction (Lisman *et al.,* 2002). AMPARp follows a similar activation profile to that of CaMKIIa but with a steeper negative slope as the simulation progresses, indicating that it is being dephosphorylated by PP1, as PP2B declines to slightly below baseline levels. Briefly sustained CaMKII activity after HFS demonstrates its activation by high levels of Ca^{2+}/calmodulin and autophosphorylation to maintain its activity (Lisman *et al.,* 2002). The initial rise in PP2B is sufficient to release the inhibition on PP1 and activate it in the model.

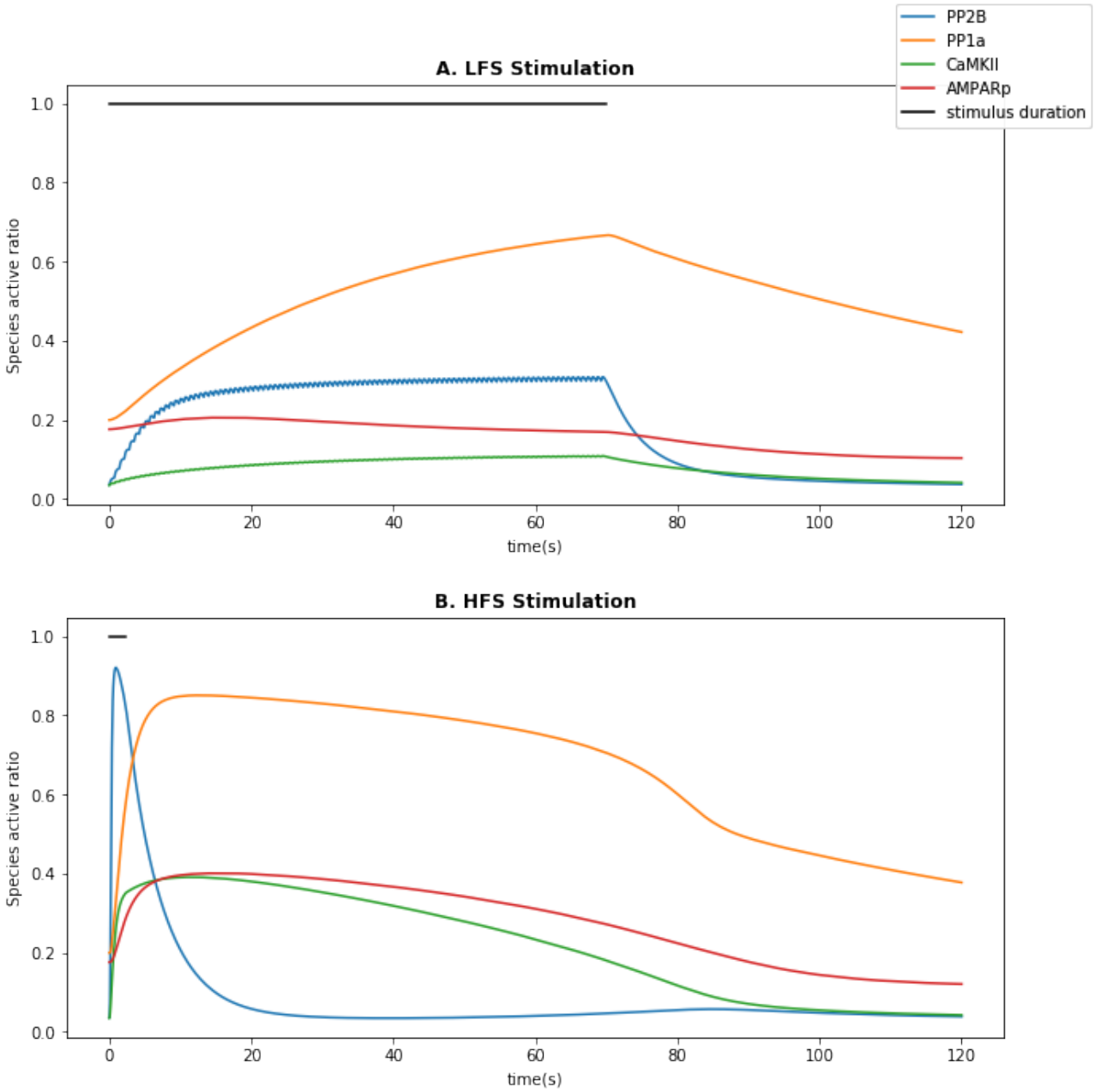

Figure 4. Enzyme activation ratio in the presence of LFS and HFS. Both plots depict the ratio of active PP2B, PP1 and CaMKII and the phosphorylation ratio of AMPARs. The ratio is computed by dividing active enzyme or phosphorylated receptor over its total concentration. Each stimulus consists of 100 Ca^{2+} spikes with equal input size as described in the methods section. (A) LFS at 1.43 Hz for 69.9s; (B) HFS at 43.73 Hz for 2.3s.

Figure 5 follows the modelling approach of Li *et al.,* (2012). The nature of plasticity, whether it is potentiation or depression, can be decoded by contrasting the activity of kinases and phosphatases. The ratio of cumulative activity of PP2B and CaMKII (Figure 5A) demonstrates that at low frequencies (< 10 Hz) PP2B activity is greater than that of CaMKII, and at higher frequencies (> 10 Hz) the opposite occurs, as the ratio shifts from being above 1 to below. This result indicates that frequencies above 10 Hz could lead to greater phosphorylation of AMPARs by CaMKIIa than dephosphorylation by PP2B, showing potentiation of the spine model. The converse occurs at frequencies below 10 Hz, suggesting spine depression.

The activity difference of kinases and phosphatases with respect to baseline frequency (0.1 Hz) (Figure 5C) was not in line with the results presented by Li *et al.,* (2012) replicated in Figure 5B. The activity difference results in Figure 5C show that all frequencies tested lead to a dominance of phosphatase activity over CaMKIIa with respect to baseline, which would lead to LTD. Figure 5B demonstrates the expected curve modelled by Li *et al*., (2012), showing a shift from LTD to LTP at 10 Hz, in accordance with Figure 5A. Nonetheless, the trend in Figure 5B was achieved by adding PP1 activity instead of subtracting it, which does not make sense theoretically, as PP1 activity opposes that of CaMKII when acting on AMPARs. This indicates that perhaps the analysis performed by Li *et al*., (2012) included an error of adding PP1 instead of subtracting it. Moreover, 120 s from stimulation start is an interesting time frame to look at initial enzyme and receptor dynamics, yet it is insufficient to model early plasticity, ranging from 1-3 hours (Baltaci *et al.,* 2019).

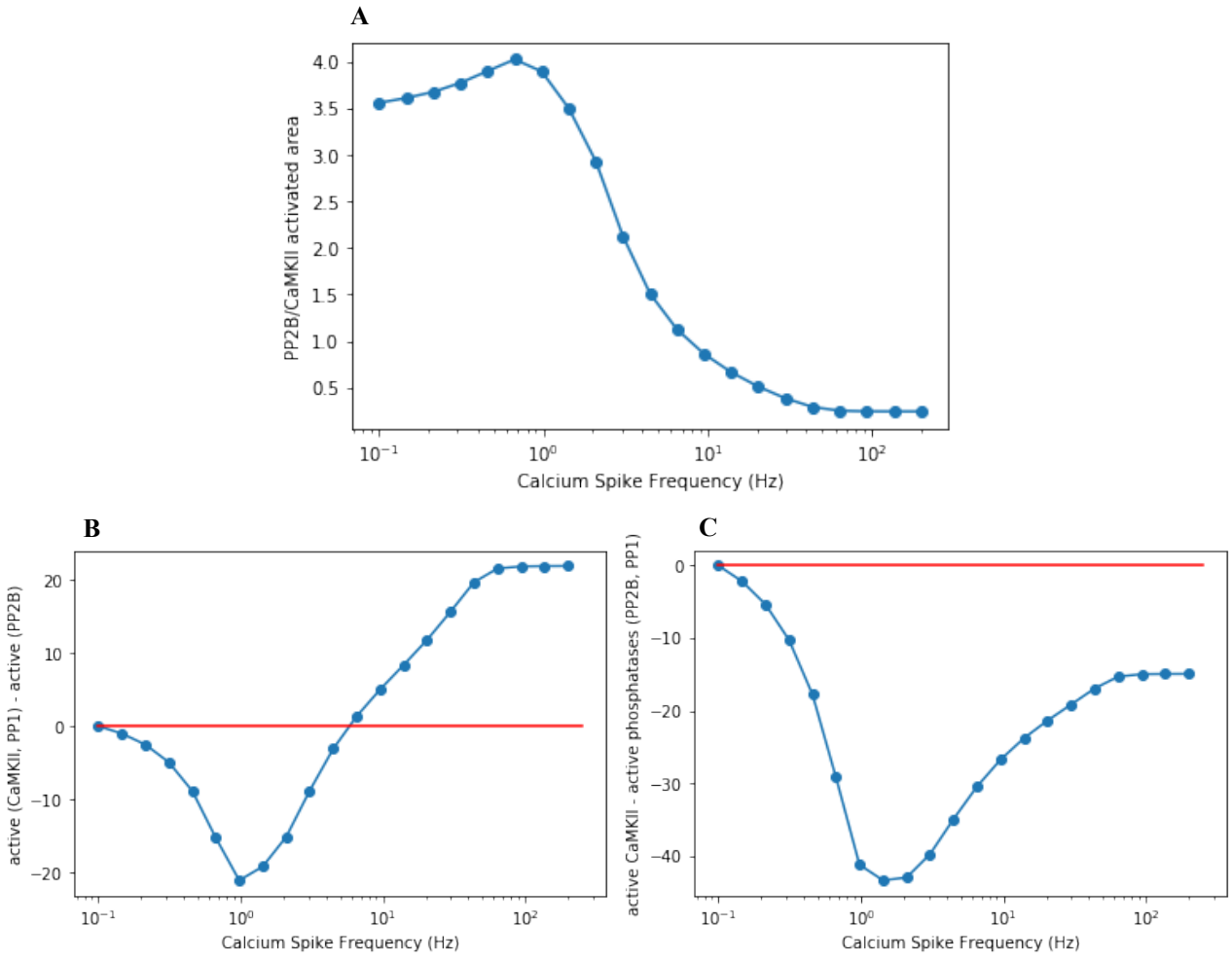

Figure 5. CaMKIIa and phosphatase (PP2B and PP1a) balance for a range of frequencies determine plasticity direction. Activated area of CaMKIIa, PP2B and PP1a is calculated as described in the methods section for all panels. Stimulation over a range of 21 frequencies, from 0.1 to 200 Hz in logarithmic scale; each frequency stimulation consists of 100 Ca^{2+} spikes. All active enzyme values are the ratio of active enzyme over total enzyme. Simulations for each individual frequency were performed for 120 s from the start of the stimulation. Values above the red line (y = 0) indicate LTP (stronger kinase activity) and below, LTD (stronger phosphatase activity). (A) Active area of calcineurin over CaMKII. (B,C) Active area of enzyme is multiplied by its k_{cat} of its reaction with the GluR1 subunit of AMPARs. (B) Activity difference as described

in the methods but with PP1 activity added instead of subtracted. (C) Activity difference calculation for the range of different frequencies as described in the methods section.

In summary, these simulations showed that the “phosphatase and kinase balance” approach to model plasticity was inconclusive and the time scale (120 s) was inaccurate. Thus, AMPAR phosphorylation was added to the model to check whether expected early plasticity behaviour could be modelled.

3.3 AMPAR phosphorylation decays quickly after stimulation

AMPAR phosphorylation was expected to stabilize for 1 hour at above or below baseline levels, after HFS or LFS respectively. Higher than baseline AMPARp ratio levels (0.176) would translate into LTP and lower into LTD.

To directly quantify AMPARp as a measure of plasticity, AMPARp ratio with respect to baseline values were recorded. AMPARp quickly decays after stimulation ceases (Figure 6A). The model’s AMPAR phosphorylation cannot be used as a direct measurement for early plasticity if it cannot replicate experimental protocols, where plasticity effects last 1-3 hours (Vertes, 2005). The dynamics of CaMKIIa as a function of time for different frequencies (Figure 6B) resemble those of AMPARp. As CaMKIIa drives AMPAR phosphorylation, a potential explanation for AMPARp values returning to baseline could stem from CaMKIIa rapidly deactivating after stimulation.

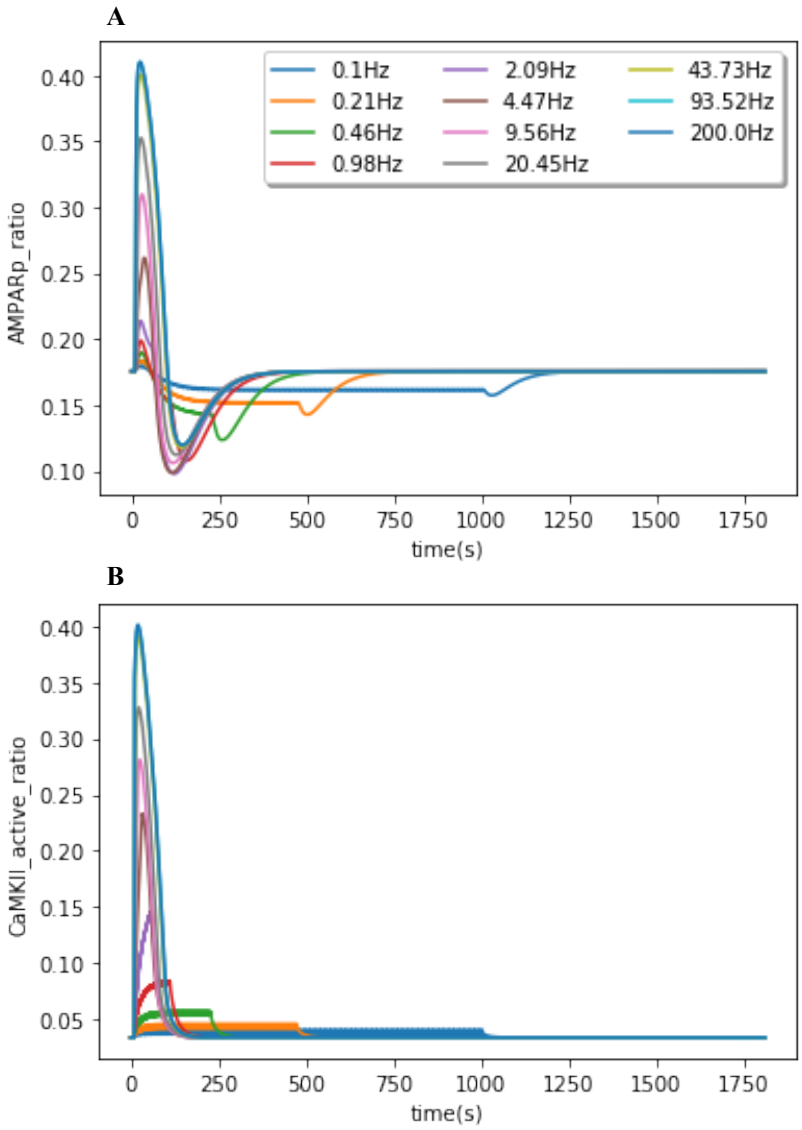

Figure 6. AMPAR phosphorylation and CaMKII activity ratio for a range of Ca^{2+} frequency stimulations. Stimulation started at 10 s and consisted of 100 spikes at different frequencies. The simulation was run for a total of 1810 s for each frequency (1800 s since stimulation starts). (A) All frequencies experience an initial rise in AMPAR phosphorylation and then decay below baseline. Eventually, AMPARp values return to baseline, indicating a gap in the ability of the model to use AMPAR phosphorylation as a readout of plasticity. (B) CaMKII activation quickly rises and then decays, demonstrating similar dynamics to those of AMPAR phosphorylation.

Four early plasticity induction protocols were tested in the model (Figure 7). AMPAR phosphorylation state was not maintained, whether it was lower than baseline (LTD) or higher (LTP). These results led to further investigation of the mechanisms governing AMPAR phosphorylation to simulate early plasticity.

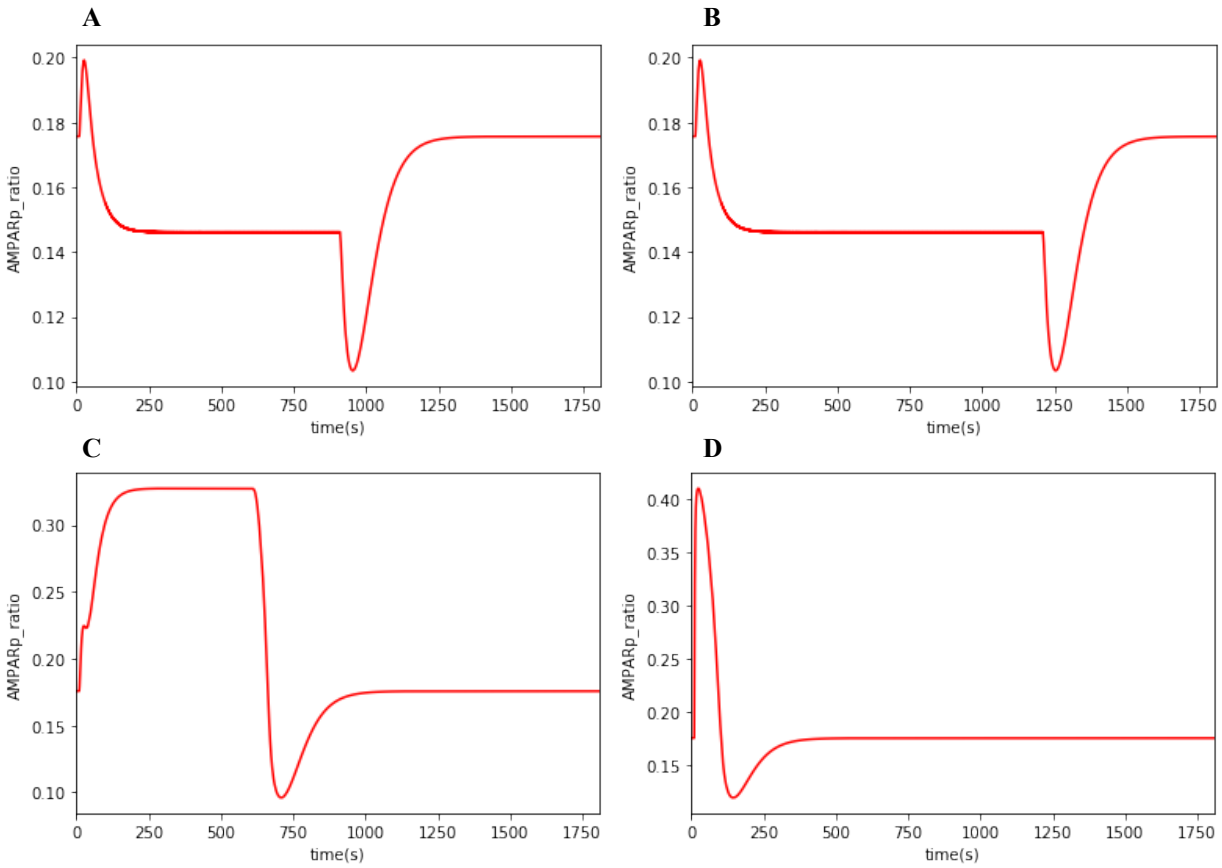

Figure 7. Early LTD and LTP experimental induction protocols applied to the model. Four experimental induction protocols were used to stimulate the spine model and AMPARp was used as a readout of plasticity, with respect to its baseline values. AMPAR phosphorylation first dropped after stimulation ended and then rose back to baseline 300 s after stimulation ended, indicating phosphorylation is not maintained and plasticity is not present. (A) 1 train of 900 spikes generated at 1 Hz; protocol by Albensi and Mattson (2000) showing LTD for 15 minutes post-stimulation in the study. (B) 1 train of 1200 spikes generated at 1Hz; protocol by Mockett *et al.,* (2002) showing LTD for 30 minutes post-stimulation in the study. (C) 1 train of 1800 spikes generated at 3 Hz; protocol by Mockett *et al.,* (2002) showing LTD for 30 minutes post-stimulation in the study. (D) 1 train of 100 spikes generated at 100 Hz; protocol by Vertes (2005) showing LTP for 1-3 hours post-stimulation in the study.

Overall, these results show that AMPAR phosphorylation is not maintained after LTP/LTD induction in the model as expected. Potentially, this issue could stem from the parameters in the model or from the experimental induction protocols not being directly translatable to the Ca^{2+} stimulation utilized. Further investigation was taken in the direction of the "inaccurate parameter" hypothesis, particularly focusing on $k_{cat}^{CaMKIIp\_PP1}$.

3.4 AMPAR phosphorylation stability: k_{cat} of PP1 dephosphorylating CaMKII

AMPAR phosphorylation maintenance could be affected by a series of modelling inaccuracies, the most obvious ones concerning phosphorylation and dephosphorylation rates of AMPARs. Results (Figure 6B) point towards CaMKII activity being short-lived, thus reducing CaMKIIa deactivation rate by PP1 should lead to sustained AMPARp and CaMKIIa levels.

In this particular model, AMPAR phosphorylation depends on CaMKII and dephosphorylation on PP1, not on PP2B directly. As PP1a acts on CaMKIIa to inactivate it, different $k_{cat}^{CaMKIIp\_PP1}$ values were examined (Figure 8). The original parameter in the model was 2.0 s^{-1} (Zhabotinsky, 2000), contrary to experimental evidence, suggesting a value of 0.043 s^{-1} (Urakubo *et al.*, 2014), that could be causing exacerbated dephosphorylation of CaMKII, leading to rapid AMPARp decay. Low $k_{cat}^{CaMKIIp\_PP1}$ values (below 0.15 s^{-1}) lead to phosphorylation of AMPARs before stimulation starts at 800 s, indicating spine excitation without a signal, that is caused by excessive CaMKIIa. Values lower than 0.15 s^{-1}, including those found by Urakubo *et al.*, (2014) would not make sense biologically in this model, indicating other model aspects should be targeted to replicate experimental results. Conversely, values of 0.5 s^{-1} and above lead to rapid decay of AMPARp to baseline, demonstrating that the rate of PP1a dephosphorylation of CaMKIIa is too strong to allow for early plasticity maintenance in the model. The results at 52.8 Hz stimulation suggest that an interesting range of $k_{cat}^{CaMKIIp\_PP1}$ values to observe would be those from 0.15 to 0.5 s^{-1} for a range of frequencies.

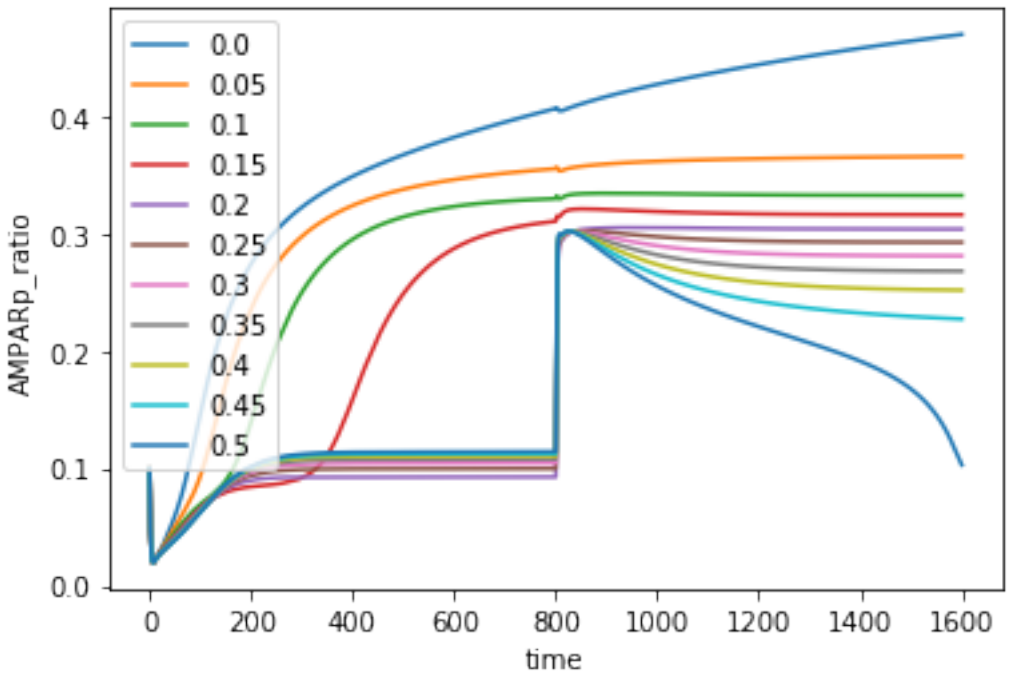

Figure 8. Analysing AMPARp stability: parameter scan for k_{cat} values of PP1 dephosphorylating CaMKII. A range of different $k_{cat}^{CaMKIIp\_PP1}$ values (0.0 to 0.5 s^{-1}) were used in individual simulations, each with 100 Ca^{2+} spikes delivered at 52.8 Hz at 800 s (equilibrium time). AMPAR phosphorylation ratio with respect to baseline was used as a readout to asses phosphorylation stability. The graph shows that for values below 0.2 s^{-1}, CaMKII activity is strong and leads to phosphorylation before stimulation, whereas for values of 0.5 s^{-1} and above (results not shown but trend observed in the model available on the GitHub repository) AMPAR phosphorylation decays back to baseline when stimulation stops.

The double parameter scan over spike frequency and $k_{cat}^{CaMKIIp\_PP1}$ values indicates that dephosphorylation of CaMKIIa by PP1a is too strong to permit activation of the kinase and, in turn, AMPAR phosphorylation for $k_{cat}^{CaMKIIp\_PP1}$ values of 0.5 s^{-1} and above, [Figure 9(A1-A3)]. Contrarily, $k_{cat}^{CaMKIIp\_PP1}$ values of 0.15 s^{-1} and below [Figure 9(B1-B3)], demonstrate elevated AMPARp and CaMKIIa baseline (0.4 for both) with respect to equilibrium values, demonstrating phosphorylation initiates before stimulation. Intermediate $k_{cat}^{CaMKIIp\_PP1}$ values, such as 0.36 s^{-1} [Figure 9(C1-C3), Table 3], show receptor, kinase and phosphatase values in LFS (0.1 and 0.46 Hz) simulations return to baseline, whereas higher frequency simulations (2.09 Hz and above), not necessarily HFS, lead to stability of AMPARp, CaMKIIa and PP1a above baseline. Furthermore, these simulations maintained the baseline of all three parameters at equilibrium levels, calculated in Figure 3, proving that there is no significant phosphorylation activity before stimulation starts. Although a difference in enzyme activation and AMPARp for LFS (e.g., 2.09 Hz) and HFS (e.g., 200 Hz) is not present, it is important to note that a first step was taken in generating two different steady states by varying $k_{cat}^{CaMKIIp\_PP1}$. Following this approach, by thoughtfully targeting other model parameters, eventually the model could exhibit different dynamics for LFS and HFS. Lastly, another issue raised by this result is the lack of LTD, where AMPARp values would be below baseline, which could perhaps be mended by adding PP2B dephosphorylation of AMPARs.

Interestingly, the dynamics of PP1a and CaMKIIa are qualitatively similar, and this is due to both quantities sharing parameters: e.g., PP1a bound to phosphorylated CaMKII would count both towards PP1a and CaMKIIa. This raises the question of whether this quantity should contribute towards phosphorylating AMPARs (CaMKIIa) or dephosphorylating AMPARs (PP1a).

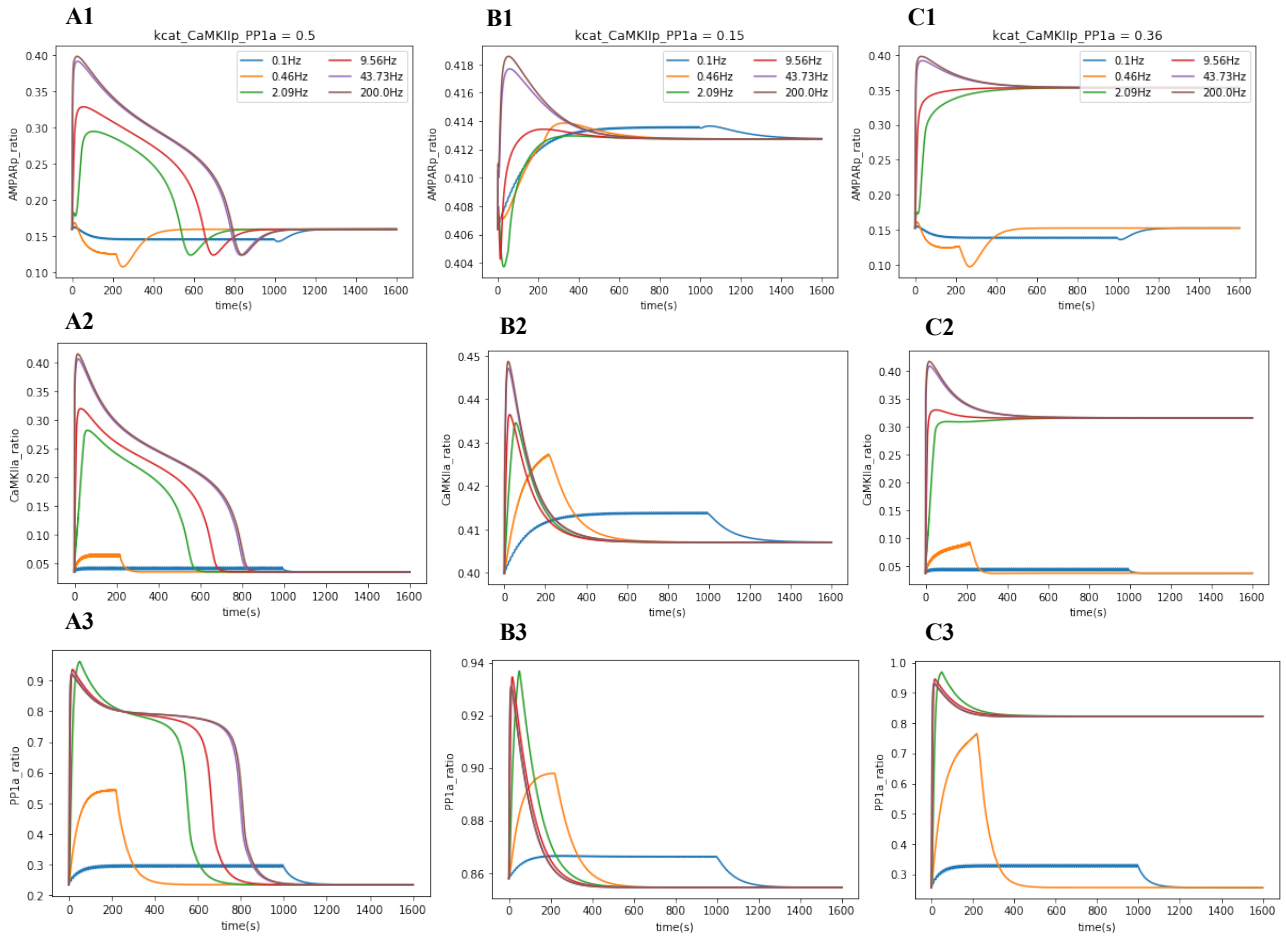

Figure 9. AMPARp, PP1a and CaMKIIa scans over spike frequency and k_{cat} of PP1a dephosphorylating CaMKIIa. All simulations are comprised of 100 Ca^{2+} spikes and stimulation starts at time = 0 s. A frequency scan was performed over six values, ranging from 0.1 to 200 Hz on a logarithmic scale, encompassing LFS and HFS values. Six different $k_{cat}^{CaMKIIp\_PP1}$ values were tested (0.15, 0.22, 0.29, 0.36, 0.43 and 0.5 s^{-1}) but only three were displayed as they covered the range of dynamics observed, the rest can be found on the GitHub repository (figures and code). (A) k_{cat} = 0.5 s^{-1}; (1-3) percent change from baseline for all frequencies: 0.00%. (B) k_{cat} = 0.15 s^{-1}; (1-3) percent change from baseline for all frequencies: 1.56% (increase), 1.79% (increase), 0.39% (decrease). (C) k_{cat} = 0.36 s^{-1}; percent change for species and frequencies in Table 3. (1) AMPAR phosphorylation ratio; (2) CaMKIIa ratio; (3) PP1a ratio.

Table 3. Initial values, final values and percent change for species in Figure 9C ($k_{cat}^{CaMKIIp\_PP1}$= 0.36 s^{-1}). The table shows the numerical values for the initial and final ratio measurements and the percent change for each species ratio at a given frequency. It is important to note, that although the percentage increase values might seem large, they concern ratio, not total values: active CaMKII did not increase by 748.19% for some frequencies, its ratio (active/total) did.

Frequency (Hz)	**Species (ratio)**					
	AMPARp		CaMKIIa		PP1a	
	Initial value = 0.15		Initial value = 0.04		Initial value = 0.26	
	Final value (1600 s)	% change	Final value (1600 s)	% change	Final value (1600 s)	% change
0.1	0.15	0.00	0.04	0.00	0.26	0.00
0.46						
2.09	0.35	132.19 (increase)	0.32	748.19% (increase)	0.82	221.14% (increase)
9.56						
43.73						
200						

To summarize, decreasing $k_{cat}^{CaMKIIp\_PP1}$, from 2.0 to (0.15-0.5 s^{-1}), triggers two equilibrium states of CaMKIIa, PP1a and AMPARp: above or at baseline. The results show the boundary of when to shift from LTD to LTP is not properly tuned. Moreover, PP1a and CaMKIIa share parameters and contribute to opposing processes. These two issues are addressed in the final modelling step taken in this dissertation.

3.5 Model Version 2: combining PP2B dephosphorylation of AMPARs with PP1a and CaMKIIa separation

The final changes added to the previously described model involved:

1. Creating two new variables: PP1a and CaMKIIa acting on AMPARs. These variables are identical to PP1a and CaMKIIa but with the shared terms removed.
2. Adding the reaction of PP2B dephosphorylating AMPARs. The reaction followed Michelis-Menten kinetics, as the reactions of PP1a and CaMKIIa with AMPARs. Table 1 shows the k_{cat} and K_M values.

Simulations using this model have not been run due to time constraints, yet both models are available on the GitHub repository, allowing for future research to perfect this model of early hippocampal plasticity.

4 Discussion

My results demonstrate that the model initially chosen requires further alteration of its parameters and reactions to achieve early plasticity dynamics. An alternative explanation for the unexpected results could be that Ca^{2+} frequency, as implemented in the model, is not the appropriate signal to mimic LTP or LTD induction. Nevertheless, the hypothesis that the interplay of CaMKII, PP1 and PP2B acting on AMPARs is sufficient to model early long-term plasticity in the hippocampus has not been disproven. The progression of the results, from looking at kinase and phosphatase balance (Figure 5), to investigating the indirect role of PP1a dephosphorylating CaMKIIa on AMPAR phosphorylation (Figure 9) demonstrates that future model variations could yield early plasticity behaviour.

The modelling approach followed throughout this dissertation (Figure 10) consisted on identifying model shortcomings after analysing a given result, in turn prompting model variations, leading to more biologically-plausible results, such as CaMKIIa bistability (Zhabotinsky, 2000; Lisman and Zhabotinsky, 2001). Consequently, three main discussion points arise:

1. Whether Ca^{2+} stimulation as implemented is a good proxy for plasticity induction.
2. The reasons for AMPARp destability or bistability and whether AMPARp is an appropriate readout of plasticity.
3. How to model SynGAP within the model, as initially proposed.

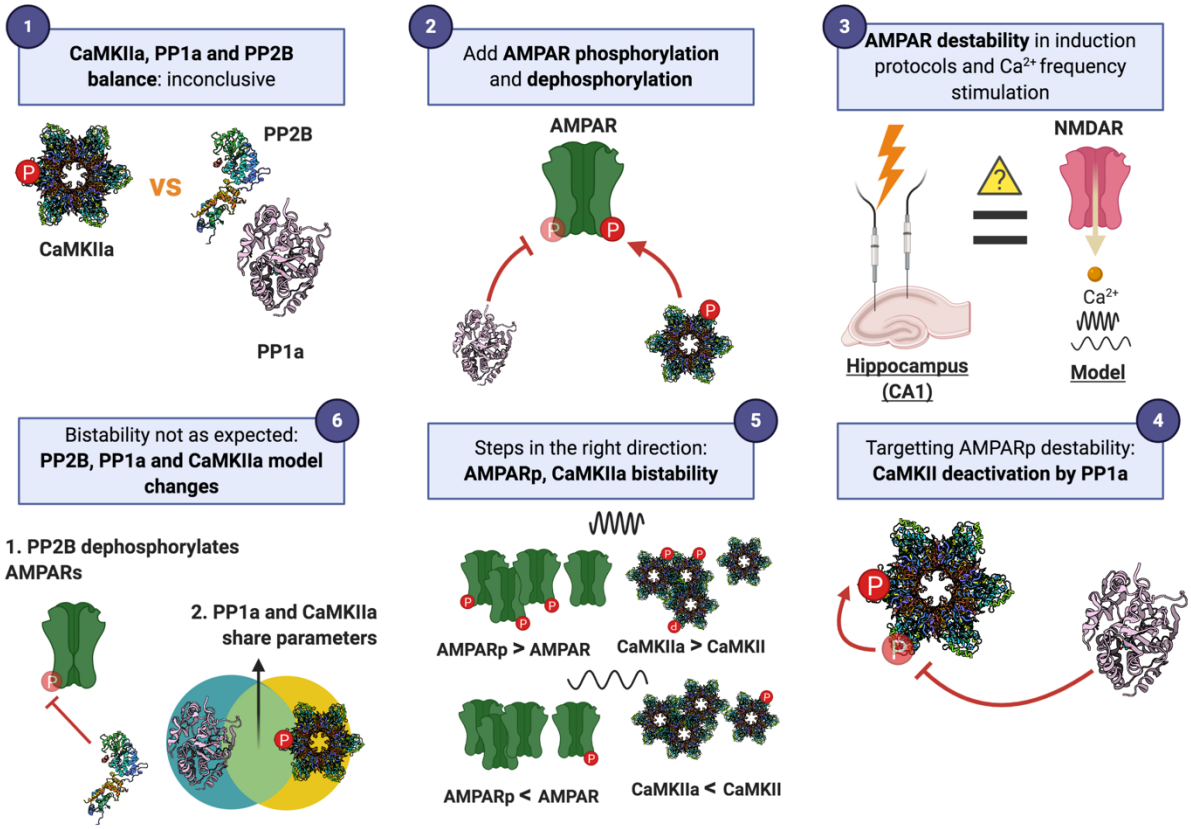

Figure 10. Experimental thought process, results summary and discussion points. The experimental protocol was constructed as results from simulations were analysed and compared to biological theory, trying to find flaws in the model to improve and reproduce early long-term potentiation. The details concerning simulations, model parameters and reactions are explained in the methods section. (1) Cumulative activity of CaMKII was compared to that of PP2B and PP1, to determine the direction of plasticity. The results contradicted those by Li *et al.,* (2012) and the simulation time (120 s) was too short to model early long-term plasticity. These inconclusive results prompted including AMPAR phosphorylation into the model (Xie *et al.*, 2019) and extending simulation time to 26 or 30 minutes. (2) AMPAR phosphorylation by CaMKIIa and dephosphorylation by PP1a was added to the model. (3) Plasticity in the model was tested by simulating a range (0.1 – 200 Hz) of Ca^{2+} stimulation frequencies. Electrophysiological induction protocols found in the literature, as mentioned in the methods section, were translated into Ca^{2+} signal frequency and tested in the model. The results showed rapid return to baseline values of CaMKIIa and AMPARp ratio, indicating that either some model parameters are incorrect or that induction of LTD and LTP in the model is not biologically accurate. Future modelling focused on the theory of some model parameters not being accurate. (4) To prolong CaMKIIa, as observed in the literature (Lisman *et al.,* 2002), the k_{cat} of PP1a dephosphorylating CaMKIIa was investigated. (5) Values of $k_{cat}^{CaMKIIp\_PP1}$ between 0.15 and 0.5 s^{-1} rendered bistability of PP1a, AMPARp and CaMKIIa. This experimental result was a step in the right direction, as achieving two states of AMPARp could explain LTD (low ratio) and LTP (high ratio). Furthermore, CaMKIIa bistability is also observed in the literature (Zhabotinsky, 2000). Nevertheless, one of the steady states was the baseline value of the species and the bistable states did not properly differentiate between LFS and HFS. Additionally, dynamics of PP1a and CaMKIIa were qualitatively similar, noting the fact that they share model terms and that they contribute to opposing processes when regarding AMPARs. (6) The final step taken was adding PP2B dephosphorylation of AMPARs, as described in the literature (Li *et al.,* 2012), hoping to achieve a below-baseline AMPARp state to model LTD. Moreover, the common terms of PP1a and CaMKIIa were removed when dealing with AMPAR phosphorylation. Due to time constraints, simulations were not run in this final model (version 2). Both models (model up to step 5 and model at step 6) are available on the GitHub repository, along with the data analysis code, making this study perfectly reproducible. Figure by author created in the BioRender App.

4.1 Calcium-dependent pathways in the hippocampal PSD

Firstly, it is important to note that the Li *et al.,* (2012) model was chosen as a starting point because of its detailed description of CaMKII autophosphorylation, calmodulin activation, phosphatase regulation and Ca^{2+} signal frequency, amplitude and duration-dependent stimulation functions.

Calcium pulses enter the postsynaptic terminal via NMDARs and the frequency, duration and amplitude of these pulses leads to differential calmodulin binding affinities (Shifman *et al.*, 2006). The structural conformation of calmodulin differs when it is Ca^{2+}-free or bound, conferring its substrate selectivity, as it binds over 300 target peptides (Westerlund and Delemotte, 2018). This model, alike Li *et al.,* (2012), builds on the Stefan *et al.,* (2008) model, assuming that the four Ca^{2+} binding sites are different and that calmodulin transitions from a low-affinity (T) to a high-affinity (R) state as Ca^{2+} binds successively. Furthermore, this approach exhibits Ca^{2+} concentration-dependent differential activation of PP2B and CaMKII by calmodulin, backed up by experimental evidence (Colbran, 2004). The accuracy of calmodulin modelling ruled it out as a model target to alter and improve.

Another advantage of the Li *et al.,* (2012) model is its elaborate calculation of CaMKII activation by autophosphorylation, as a function of active CaMKII monomers. Nevertheless, this activation pathway causes CaMKIIa to rapidly return to baseline values when stimulation ends (Figure 6B), contradicting biological studies where CaMKII activity is sustained an hour after plasticity induction (Lisman *et al.,* 2002). This issue could be caused by excessive CaMKIIa dephosphorylation by PP1a, concluding that decreasing the rate of this reaction (Figure 9) leads to biologically-plausible CaMKII activity and bistability as in the literature (Lisman and Zhabotinsky, 2001). An in-vitro study suggests this catalytic constant equals 0.043 s^{-1}, whereas this study shows that values below 0.15 s^{-1} render AMPAR phosphorylation increase before stimulation, which is not biologically accurate. It is plausible that the higher value range is a compensatory mechanism for low levels of AMPAR dephosphorylation.

4.2 AMPAR phosphorylation as a readout of plasticity

This dissertation focused on AMPAR GluR1 subunit phosphorylation as a readout of plasticity, where above baseline levels were considered as LTP and below as LTD. These dynamics are partially achieved (Figure 9C), yet AMPARp bistability does not discriminate properly between LFS and HFS and no LTD is observed. These results suggest a potential deficiency in AMPAR dephosphorylation. By running simulations on the second version of the model, that includes dephosphorylation of AMPARs by PP2B, stable below-baseline results could potentially be induced.

Mutations in GluR1 phosphorylation sites, phosphorylated by PKA and CaMKII and dephosphorylated by PP2B and PP1, demonstrated impaired LTD and LTP (Lee *et al.*, 2003). Other studies suggest that phosphorylation affects AMPAR conductance and plasticity expression, but that it is not crucial for its induction (Huganir and Nicoll, 2013). The most accurate readout of plasticity studied is AMPAR trafficking to and from the synapse (Anggono and Huganir, 2012). AMPARs maintain plasticity by undergoing exocytosis and endocytosis near the synapse and then travelling to the PSD by lateral diffusion (Anggono and Huganir, 2012). Particularly, phosphorylation of GluR1 (Ser845) by PKA, together with CaMKII activity, in the rat hippocampus mediates AMPAR trafficking into the PSD (Esteban *et al.*, 2003). Taking advantage of PKA's presence in the model, these experiments suggest AMPAR trafficking could be included, together with AMPAR phosphorylation, to model plasticity more accurately.

4.3 Model limitations and future directions

The main drawback of this model lies in its inability to demonstrate frequency-dependent AMPAR phosphorylation that adheres to experimental induction protocols: LFS driving LTD and HFS generating LTP. The model insufficiency gives rise to three main limitations and future avenues to explore: (i) insufficient dephosphorylation of AMPARs; (ii) AMPARp as a readout of early hippocampal plasticity; (iii) Ca^{2+} frequency as an induction signal of plasticity.

The lack of stable below-baseline levels of AMPARp, as shown in Figure 6, 7 and 9, demonstrate that perhaps the dephosphorylation rate of AMPARs by PP1a is insufficient. To mend this problem, the second version of the model was created, including AMPAR dephosphorylation by PP2B. Experiments that could be run in the near-future would involve performing the same simulations in this study on the new model version. Furthermore, parameter scans of the k_{cat} for the dephosphorylation of AMPARs by PP2B and PP1a could be explored.

From reviewing the literature, it has become evident that AMPAR phosphorylation itself might be insufficient to model early plasticity, pointing to the incorporation of AMPAR trafficking in future model versions. AMPAR trafficking would require the addition of an independent variable: space. To achieve a spatial model, that takes into account AMPAR diffusion rates, the reactions would have to be modelled as a function of time and space, achieved by using partial differential equations (PDEs) as opposed to ODEs. This model would be ideal to build upon by adding SynGAP mechanisms to study disease.

Time limitations did not allow to test disease modelling, which aimed to focus on SynGAP KO modelling. Theoretically, this pathway could have been added to the model without major alterations, as SynGAP is closely associated with NMDARs and is regulated by CaMKII (Gamache *et al.,* 2020).

SynGAP phosphorylation by CaMKII causes its dispersion from the synapse, leading to LTP by AMPAR trafficking and clustering at the synapse (Araki *et al.*, 2015). Heterozygote KO SynGAP mice show excessive AMPAR clustering and deficits in LTP but not LTD at hippocampal synapses (Kim *et al.*, 2003), suggesting that the stimulus needed to induce LTP is greater. SynGAP dispersion could be modelled as a function of CaMKII activity, making SynGAP concentration inversely proportional to AMPAR trafficking and number. The model extension could be validated by testing literature LTP induction protocols applied to SynGAP KO mice (Komiyama *et al.*, 2002) and comparing the results.

Finally, it is unclear whether Ca^{2+} frequency stimulation, as used in this study, can act as a proxy for experimental plasticity induction, as experimental induction is never performed at the spine-level. This question would shift the nature of the investigation from biochemical to electrophysiological. As a starting point, spike-timing dependent plasticity could be modelled by adding a presynaptic spine and the results of the simulations could be tested experimentally using electrophysiology and Ca^{2+} imaging.

5 Conclusions

The beauty of modelling lies in its efficiency to test hypothesis by running simulations, elucidating biological behaviour, and then generating predictions to test experimentally. In conclusion, the initial hypothesis that kinase and phosphatase activity on AMPARs is sufficient to model homosynaptic hippocampal early plasticity has not been disproven. This hippocampal early plasticity model demonstrates that kinases and phosphatases can be used to model bistable AMPAR phosphorylation as a function of Ca^{2+} frequency stimulation. AMPAR phosphorylation dynamics, controlled directly by PP1a and CaMKIIa, demonstrate above-baseline stability for Ca^{2+} frequencies of 2.09 Hz and above, and baseline stability for frequencies of 0.46 Hz and below. This bistability separation is inconsistent with HFS triggering LTP and LFS prompting LTD. Nevertheless, this model demonstrates the potential to achieve early plasticity behaviour if future research into dephosphorylation parameters is undertaken, following a similar modelling approach as the one in this study.

Acknowledgements

I would like to thank both my supervisors, Dr. Matthias Hennig and Dr. Melanie Stefan, for not only guiding me, but challenging me and making this dissertation very intellectually rewarding. Furthermore, I would also like to thank Dr. Emily Osterweil for her advice and knowledge on SynGAP modelling.

Finally, I would like to thank my flatmates, Ms. Azucena Garvia, Ms. Patricia Diana and Ms. Irati Colmenero, for their constant encouragement and making the writing of this dissertation fun during this isolation period.

References

Abbott, L. F. and Nelson, S. B. (2000) ‘Synaptic plasticity: taming the beast’, *Nature Neuroscience*, 3(11), pp. 1178–1183. doi: 10.1038/81453.

Albensi, B. C. *et al.* (2007) ‘Electrical stimulation protocols for hippocampal synaptic plasticity and neuronal hyper-excitability: Are they effective or relevant?’, *Experimental Neurology*, 204(1), pp. 1–13. doi: https://doi.org/10.1016/j.expneurol.2006.12.009.

Albensi, B. C. and Mattson, M. P. (2000) ‘Evidence for the involvement of TNF and NF-κB in hippocampal synaptic plasticity’, *Synapse*. John Wiley & Sons, Ltd, 35(2), pp. 151–159. doi: 10.1002/(SICI)1098-2396(200002)35:2<151::AID-SYN8>3.0.CO;2-P.

Anggono, V. and Huganir, R. L. (2012) ‘Regulation of AMPA receptor trafficking and synaptic plasticity’, *Current opinion in neurobiology*. 2012/01/02, 22(3), pp. 461–469. doi: 10.1016/j.conb.2011.12.006.

Antunes, G. and Simoes-de-Souza, F. M. (2018) ‘AMPA receptor trafficking and its role in heterosynaptic plasticity’, *Scientific Reports*, 8(1), p. 10349. doi: 10.1038/s41598-018-28581-w.

Araki, Y. *et al.* (2015) ‘Rapid dispersion of SynGAP from synaptic spines triggers AMPA receptor insertion and spine enlargement during LTP’, *Neuron*, 85(1), pp. 173–189. doi: 10.1016/j.neuron.2014.12.023.

Baltaci, S. B., Mogulkoc, R. and Baltaci, A. K. (2019) ‘Molecular Mechanisms of Early and Late LTP’, *Neurochemical Research*, 44(2), pp. 281–296. doi: 10.1007/s11064-018-2695-4.

Barria, A., Derkach, V. and Soderling, T. (1997) ‘Identification of the Ca2+/calmodulin-dependent protein kinase II regulatory phosphorylation site in the alpha-amino-3-hydroxyl-5-methyl-4-isoxazole-propionate-type glutamate receptor.’, *The Journal of biological chemistry*. United States, 272(52), pp. 32727–32730. doi: 10.1074/jbc.272.52.32727.

Chistiakova, M. *et al.* (2015) ‘Homeostatic role of heterosynaptic plasticity: models and experiments ’, *Frontiers in Computational Neuroscience* , p. 89. Available at: https://www.frontiersin.org/article/10.3389/fncom.2015.00089.

Citri, A. and Malenka, R. C. (2008) ‘Synaptic Plasticity: Multiple Forms, Functions, and Mechanisms’, *Neuropsychopharmacology*, 33(1), pp. 18–41. doi: 10.1038/sj.npp.1301559.

Colbran, R. J. (2004) ‘Protein Phosphatases and Calcium/Calmodulin-Dependent Protein

Kinase II-Dependent Synaptic Plasticity', *The Journal of Neuroscience*, 24(39), pp. 8404 LP – 8409. doi: 10.1523/JNEUROSCI.3602-04.2004.

Esteban, J. A. *et al.* (2003) 'PKA phosphorylation of AMPA receptor subunits controls synaptic trafficking underlying plasticity', *Nature Neuroscience*, 6(2), pp. 136–143. doi: 10.1038/nn997.

Gamache, T. R., Araki, Y. and Huganir, R. L. (2020) 'Twenty Years of SynGAP Research: From Synapses to Cognition', *The Journal of Neuroscience*, 40(8), pp. 1596 LP – 1605. doi: 10.1523/JNEUROSCI.0420-19.2020.

Gladding, C. M., Fitzjohn, S. M. and Molnár, E. (2009) 'Metabotropic glutamate receptor-mediated long-term depression: molecular mechanisms', *Pharmacological reviews*. 2009/11/19. The American Society for Pharmacology and Experimental Therapeutics, 61(4), pp. 395–412. doi: 10.1124/pr.109.001735.

Hayer, A. and Bhalla, U. S. (2005) 'Molecular Switches at the Synapse Emerge from Receptor and Kinase Traffic', *PLOS Computational Biology*. Public Library of Science, 1(2), p. e20. Available at: https://doi.org/10.1371/journal.pcbi.0010020.

Hoops, S. *et al.* (2006) 'COPASI—a COmplex PAthway SImulator', *Bioinformatics*, 22(24), pp. 3067–3074. doi: 10.1093/bioinformatics/btl485.

Huganir, R. L. and Nicoll, R. A. (2013) 'AMPARs and Synaptic Plasticity: The Last 25 Years', *Neuron*, 80(3), pp. 704–717. doi: https://doi.org/10.1016/j.neuron.2013.10.025.

Kaizuka, T. and Takumi, T. (2018) 'Postsynaptic density proteins and their involvement in neurodevelopmental disorders', *The Journal of Biochemistry*, 163(6), pp. 447–455. doi: 10.1093/jb/mvy022.

Kim, J. H. *et al.* (2003) 'The role of synaptic GTPase-activating protein in neuronal development and synaptic plasticity', *The Journal of neuroscience : the official journal of the Society for Neuroscience*. Society for Neuroscience, 23(4), pp. 1119–1124. doi: 10.1523/JNEUROSCI.23-04-01119.2003.

Kim, S. and Ziff, E. B. (2014) 'Calcineurin mediates synaptic scaling via synaptic trafficking of Ca2+-permeable AMPA receptors', *PLoS biology*. Public Library of Science, 12(7), pp. e1001900–e1001900. doi: 10.1371/journal.pbio.1001900.

Komiyama, N. H. *et al.* (2002) 'SynGAP Regulates ERK/MAPK Signaling, Synaptic Plasticity, and Learning in the Complex with Postsynaptic Density 95 and NMDA Receptor',

The Journal of Neuroscience, 22(22), pp. 9721 LP – 9732. doi: 10.1523/JNEUROSCI.22-22-09721.2002.

Lee, H.-K. *et al.* (2003) 'Phosphorylation of the AMPA Receptor GluR1 Subunit Is Required for Synaptic Plasticity and Retention of Spatial Memory', *Cell*. Elsevier, 112(5), pp. 631–643. doi: 10.1016/S0092-8674(03)00122-3.

Li, L., Stefan, M. I. and Le Novère, N. (2012) 'Calcium Input Frequency, Duration and Amplitude Differentially Modulate the Relative Activation of Calcineurin and CaMKII', *PLOS ONE*. Public Library of Science, 7(9), p. e43810. Available at: https://doi.org/10.1371/journal.pone.0043810.

Lisman, J. E. and Zhabotinsky, A. M. (2001) 'A Model of Synaptic Memory: A CaMKII/PP1 Switch that Potentiates Transmission by Organizing an AMPA Receptor Anchoring Assembly', *Neuron*. Elsevier, 31(2), pp. 191–201. doi: 10.1016/S0896-6273(01)00364-6.

Lisman, J., Schulman, H. and Cline, H. (2002) 'The molecular basis of CaMKII function in synaptic and behavioural memory', *Nature Reviews Neuroscience*, 3(3), pp. 175–190. doi: 10.1038/nrn753.

Malenka, R. C. and Nicoll, R. A. (1993) 'NMDA-receptor-dependent synaptic plasticity: multiple forms and mechanisms', *Trends in Neurosciences*, 16(12), pp. 521–527. doi: https://doi.org/10.1016/0166-2236(93)90197-T.

Mockett, B., Coussens, C. and Abraham, W. C. (2002) 'NMDA receptor-mediated metaplasticity during the induction of long-term depression by low-frequency stimulation', *European Journal of Neuroscience*. John Wiley & Sons, Ltd, 15(11), pp. 1819–1826. doi: 10.1046/j.1460-9568.2002.02008.x.

Mulkey, R. M. *et al.* (1994) 'Involvement of a calcineurin/ inhibitor-1 phosphatase cascade in hippocampal long-term depression', *Nature*, 369(6480), pp. 486–488. doi: 10.1038/369486a0.

Nicoll, R. A., Tomita, S. and Bredt, D. S. (2006) 'Auxiliary Subunits Assist AMPA-Type Glutamate Receptors', *Science*, 311(5765), pp. 1253 LP – 1256. doi: 10.1126/science.1123339.

Piochon, C., Kano, M. and Hansel, C. (2016) 'LTD-like molecular pathways in developmental synaptic pruning', *Nature Neuroscience*, 19(10), pp. 1299–1310. doi: 10.1038/nn.4389.

Schonewille, M. *et al.* (2010) 'Purkinje cell-specific knockout of the protein phosphatase

PP2B impairs potentiation and cerebellar motor learning', *Neuron*, 67(4), pp. 618–628. doi: 10.1016/j.neuron.2010.07.009.

Shifman, J. M. *et al.* (2006) 'Ca2+/calmodulin-dependent protein kinase II (CaMKII) is activated by calmodulin with two bound calciums', *Proceedings of the National Academy of Sciences*, 103(38), pp. 13968 LP – 13973. doi: 10.1073/pnas.0606433103.

Stefan, M. I., Edelstein, S. J. and Le Novère, N. (2008) 'An allosteric model of calmodulin explains differential activation of PP2B and CaMKII', *Proceedings of the National Academy of Sciences*, 105(31), pp. 10768 LP – 10773. doi: 10.1073/pnas.0804672105.

Urakubo, H. *et al.* (2014) 'In Vitro Reconstitution of a CaMKII Memory Switch by an NMDA Receptor-Derived Peptide', *Biophysical Journal*. Elsevier, 106(6), pp. 1414–1420. doi: 10.1016/j.bpj.2014.01.026.

Vertes, R. P. (2005) 'Hippocampal theta rhythm: A tag for short-term memory', *Hippocampus*. John Wiley & Sons, Ltd, 15(7), pp. 923–935. doi: 10.1002/hipo.20118.

Wang, C.-C., Held, R. G. and Hall, B. J. (2014) 'SynGAP Regulates Protein Synthesis and Homeostatic Synaptic Plasticity in Developing Cortical Networks', *PLOS ONE*. Public Library of Science, 8(12), p. e83941. Available at: https://doi.org/10.1371/journal.pone.0083941.

Westerlund, A. M. and Delemotte, L. (2018) 'Effect of Ca2+ on the promiscuous target-protein binding of calmodulin', *PLOS Computational Biology*. Edited by R. Nussinov. Public Library of Science, 14(4), p. e1006072. doi: 10.1371/journal.pcbi.1006072.

Woolfrey, K. M. and Dell'Acqua, M. L. (2015) 'Coordination of Protein Phosphorylation and Dephosphorylation in Synaptic Plasticity', *The Journal of biological chemistry*. 2015/10/09. American Society for Biochemistry and Molecular Biology, 290(48), pp. 28604–28612. doi: 10.1074/jbc.R115.657262.

Xie, Y. *et al.* (2019) 'A multi-scale model reveals cellular and physiological mechanisms underlying hyperpolarisation-gated synaptic plasticity', *bioRxiv*, p. 418228. doi: 10.1101/418228.

Zhabotinsky, A. M. (2000) 'Bistability in the Ca2+/Calmodulin-Dependent Protein Kinase-Phosphatase System', *Biophysical Journal*, 79(5), pp. 2211–2221. doi: https://doi.org/10.1016/S0006-3495(00)76469-1.